

# The spatial response function of SeaWinds backscatter measurements

Ivan S. Ashcraft and David G. Long

Brigham Young University, 459 Clyde Building, Provo, UT 84602, USA

## ABSTRACT

Designed to retrieve near-surface winds over the ocean, the SeaWinds scatterometer makes 13.4 GHz Ku-band measurements of the normalized radar backscatter of the Earth's surface. SeaWinds backscatter measurements are being used in a wide variety of studies, including ocean wind retrieval, sea-ice mapping and classification, iceberg tracking, vegetation, soil moisture, and snow accumulation. Two SeaWinds instruments are currently flying in orbit.

Due to the high spatial sampling density, SeaWinds data is ideally suited for the application of reconstruction and resolution enhancement algorithms. Such algorithms require accurate knowledge of the spatial response function of the individual measurements, "slices" and "eggs". Standard SeaWinds data products from JPL include the locations of the measurements, but not the response functions. In this paper we derive the spatial response function for both egg and slices. The response functions vary with antenna azimuth and orbit location. Because computation of the response function is laborious, methods of tabularizing and interpolating the response function have been developed. These are described in this paper. We provide code and the tables to enable computation the response function using information from standard JPL data products. We hope these will further the development of resolution-enhanced SeaWinds data. Examples of resulting enhanced resolution images are included.

**Keywords:** scatterometer, SeaWinds, radar backscatter, ocean winds, QuikSCAT, radar equation

## 1. INTRODUCTION

The first pencil-beam scatterometer, the Ku-band SeaWinds scatterometer, was launched in July 1999 aboard the QuikSCAT satellite. A second SeaWinds instrument was launched aboard the Japanese Advanced Earth Observing System-II (ADEOS-II) in December 2002. Both instruments are now operating. SeaWinds is designed to measure the normalized radar backscatter ( $\sigma^0$ ) of the Earth's surface at two incidence angles and two polarizations (H-pol at  $46^\circ$ , and V-pol at  $54^\circ$ ) with a diversity of azimuth angles. From these measurements the near-surface vector wind can be estimated over the ocean.<sup>1</sup> SeaWinds observes over 90% of the ocean's surface each day. Because wind modulates all air-sea fluxes, this data is important in weather prediction and air-sea interaction studies. Measurements are also collected over the land and ice areas of the Earth. SeaWinds  $\sigma^0$  measurements over these land and ice regions are used to produce images of the Earth's land and ice surfaces to support climate studies and monitor the Cryosphere.<sup>2</sup> Currently, in addition to ocean wind measurement, SeaWinds data is being operationally used in sea-ice mapping and iceberg tracking.

SeaWinds imaging applications are facilitated by applying reconstruction and resolution enhancement algorithms such as the Scatterometer Image Reconstruction (SIR) algorithm.<sup>3,4</sup> Application of SIR and other imaging algorithms require knowledge of the spatial response function (also called the aperture or point spread function) of the measurements. The pencil beam design and onboard processing result in a spatial response function which varies between individual measurements and is a function of orbital position and antenna rotation angle.

---

Further author information: (Send correspondence to DGL)

ISA: E-mail: ashcraft@ee.byu.edu, Telephone: 1 801 422 4884

DGL: E-mail: long@ee.byu.edu, Telephone: 1 801 422 4383

In this paper we describe how the spatial response function for a given SeaWinds measurement is computed. This calculation is too computationally intensive to be performed in real time, requiring that it be precomputed and tabularized as a function of antenna beam, antenna rotation angle, and orbit position. We describe the tabularization method. The tables and code are available from the Scatterometer Climate Record Pathfinder (SCP) web/ftp site at <http://www.scp.byu.edu>. We hope that making the SeaWinds response function more widely available will increase the application of SeaWinds data in high resolution studies of the Earth. Note that the SCP has a wide compilation of existing SeaWinds imagery available.<sup>2</sup> Section 2 provides essential background and describes the computation of the spatial response function. Section 3 describes how the spatial response function is tabularized. Section 4 provides some examples of how the spatial response function is used in creating enhanced resolution  $\sigma^\circ$  images from the low resolution measurements. A summary conclusion is provided in Section 5.

## 2. THE SEAWINDS SPATIAL RESPONSE FUNCTION

Operating at 13.4 GHz, the SeaWinds scatterometer transmits nominally 0.5 ms microwave pulses at a pulse rate of 192 Hz using a dual-beam conically rotating dish antenna. The antenna rotates at approximately 18 rpm about the nadir vector. The radar transmits alternately on each of two beams. These beams trace out a helix on the earth as the satellite passes overhead.<sup>5</sup> The inner beam transmits and receives horizontally-polarized microwave signals while the outer beam transmits and receives vertically-polarized signals. The radar echo from the surface is received and processed to compute the  $\sigma^\circ$  of the illuminated area. The two-way 3 dB antenna footprint is elliptically shaped with dimensions of approximately 25 km by 35 km. The SeaWinds measurement of this area is termed an “egg”. The 110 W peak power transmit signal is chirped, with a bandwidth of 160 kHz. The Doppler shift ( $\pm 500$  kHz, depending on antenna rotation angle and orbit position) is pre-compensated for by adjusting the transmit center frequency as a function of antenna rotation angle and orbit position so that the received echo center frequency is fixed. An onboard digital signal processor uses range filtering to divide the return echo into multiple range bins (termed “slices”), of which eight are retained and transmitted to the ground. The digital processor has eight different operational modes which adjust the width of the slices by altering the transmit pulse length. The nominal operation mode results in slices with corresponding dimensions of approximately 6 km by 25 km.

The spatial response function is the contribution of each point on the surface to the overall backscatter measurement as given in the integral form of the radar equation.<sup>6</sup> For SeaWinds the received power is

$$P_r = P_t \frac{\lambda^2}{(4\pi)^3} \int_F \frac{G^2 G_F \sigma^\circ}{R^4} dA \quad (1)$$

where  $P_r$  is the return power,  $P_t$  is the transmit power,  $\lambda$  is the wavelength,  $G$  is the antenna gain,  $\sigma^\circ$  is the normalized radar cross-section, and  $R$  is the slant range.  $F$  denotes the complete illuminated area with non-negligible gain. The  $G_F$  term is specific to SeaWinds and represents the slice- or egg-dependent gain of the digital processor. For an individual backscatter measurement,  $\sigma^\circ$  is assumed constant over the illuminated area. Incorporating this assumption into Eq. 1 and solving for  $\sigma^\circ$  yields

$$\hat{\sigma}^\circ = \frac{P_r (4\pi)^3}{P_t \lambda^2} \bigg/ \int_F \frac{G^2 G_F}{R^4} dA \quad (2)$$

$$= P_r / X \quad (3)$$

where the notation  $\hat{\sigma}^\circ$  is used to distinguish the satellite estimate of the backscatter from the actual  $\sigma^\circ$  which is spatially variant across the footprint and  $X$  contains parameters of the radar equation,

$$X = \frac{P_t \lambda^2}{(4\pi)^3} \int_F \frac{G^2 G_F}{R^4} dA. \quad (4)$$

Substituting Eq. 1 into Eq. 2 yields

$$\hat{\sigma}^\circ = \frac{\int_F (G^2 G_F \sigma^\circ) / R^4 dA}{\int_F (G^2 G_F) / R^4 dA}. \quad (5)$$

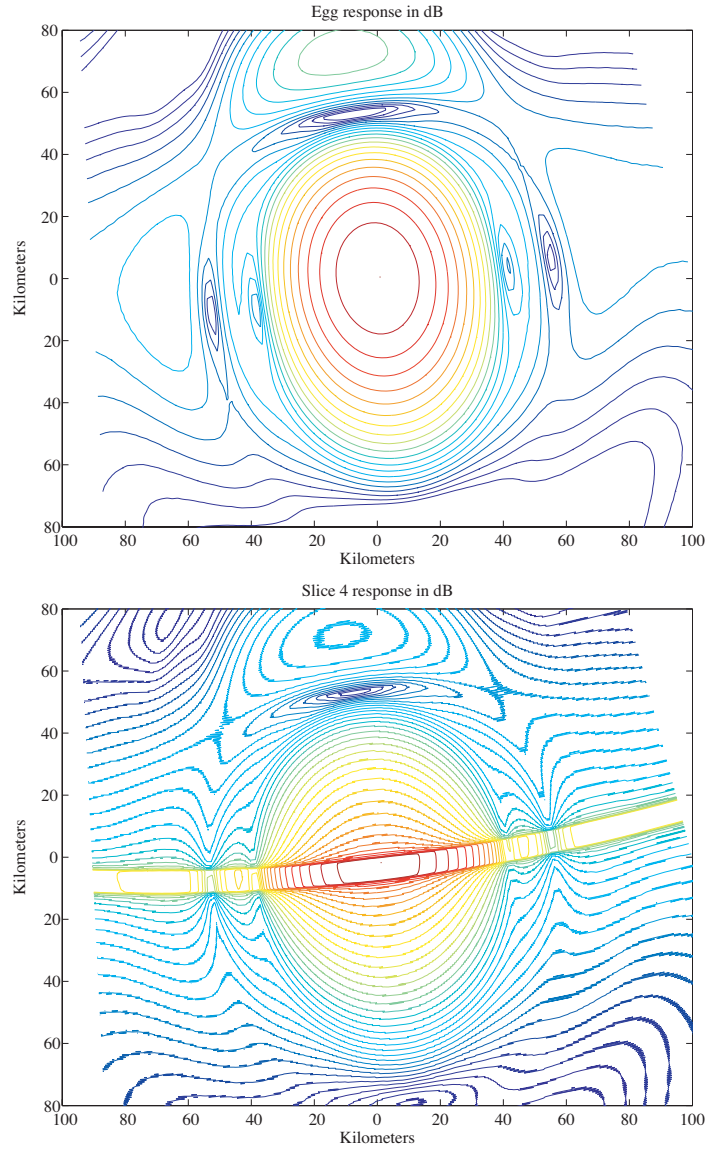


**Figure 1.** The spatial response function of an “egg” and a “slice” (slice 4) for a typical SeaWinds measurement plotted on a kilometer grid. The shapes and orientations vary with antenna azimuth angle and orbit position, as well as slice number in the slice case. Contours are spaced at 3 dB with highest contour 3 dB down from the peak.

Thus  $\hat{\sigma}^\circ$  is a weighted average of  $\sigma^\circ$  over the illuminated area with a weighting function  $h' = (G^2 G_F)/R^4$ . In effect, this weighting function is the spatial response function. Normalizing, the spatial response function  $h$  is defined as  $h = h'/h_0$  so that

$$\iint h(x, y) dx dy = 1 \quad (6)$$

where  $x, y$  represent a suitably defined coordinate system and

$$h_0 = \iint \frac{G^2(x, y) G_F(x, y)}{R^4(x, y)} dx dy. \quad (7)$$

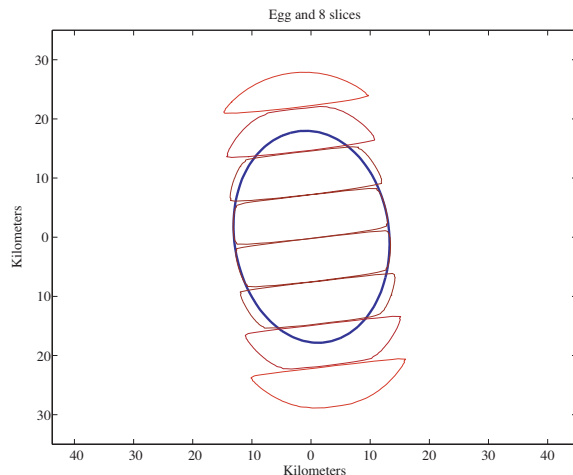


**Figure 2.** The 3 dB contours of the “egg” (thick line) and eight “slices” (thin lines) for a typical SeaWinds measurement plotted on a kilometer grid.

The integration is performed over the area for which  $G^2(x, y)G_F(x, y)$  is non-negligible. We note that while  $G$  is fixed, the  $x, y$  coordinate mapping varies with the antenna rotation angle, orbit position, and beam.  $G_F$  varies with the antenna rotation angle, orbit position, beam, and slice number.<sup>7</sup> Note that

$$X = \frac{P_t \lambda^2}{(4\pi)^3} \iint h'(x, y) dx dy \quad (8)$$

$$= \frac{P_t \lambda^2}{(4\pi)^3} h_0 \iint h(x, y) dx dy. \quad (9)$$

A given  $\sigma^\circ$  observation  $\hat{\sigma}^\circ$  can thus be written as convolution of the surface  $\sigma^\circ$  with the spatial response or point spread function  $h(x, y)$ , i.e.,

$$\hat{\sigma}^\circ = \iint h(x, y) \sigma^\circ(x, y) dx dy. \quad (10)$$

Figure 1 illustrates  $h$  for a particular egg and slice. Figure 2 illustrates the 3 dB contours of  $h$  for a particular egg and its corresponding slices.

### 3. TABULATING THE RESPONSE FUNCTION

The primary application of the spatial response function  $h$  is image reconstruction. Image reconstruction is a basic inverse convolution problem which takes advantage of overlapping  $\sigma^\circ$  measurements resulting in increased spatial resolution.<sup>3</sup> The accuracy of the reconstructed image depends on accurate knowledge of the response function. However, there is a tradeoff between accuracy, computation requirements, and effective resolution of the reconstructed image. Due to the rapid rolloff and nearly flat mainlobe response of the slices, a significant savings in complexity and computation can be obtained, with only a minor loss in image quality, by quantizing  $h(x, y)$  to either 1 or 0. Hence, only the shape of the 3 dB contour is required to describe  $h(x, y)$  for slices. Since the spatial rolloff of  $h(x, y)$  for egg measurements is much slower, this approximation for eggs leads to excessive error. Instead, the full range of values for  $h(x, y)$  is retained\*.

---

\*As noted by Early and Long<sup>3</sup> the spatial response function for the NASA Scatterometer (NSCAT) can be similarly quantized while the ERS-1/2 scatterometer response is generally not quantized for the same reasons the SeaWinds egg response is not quantized.

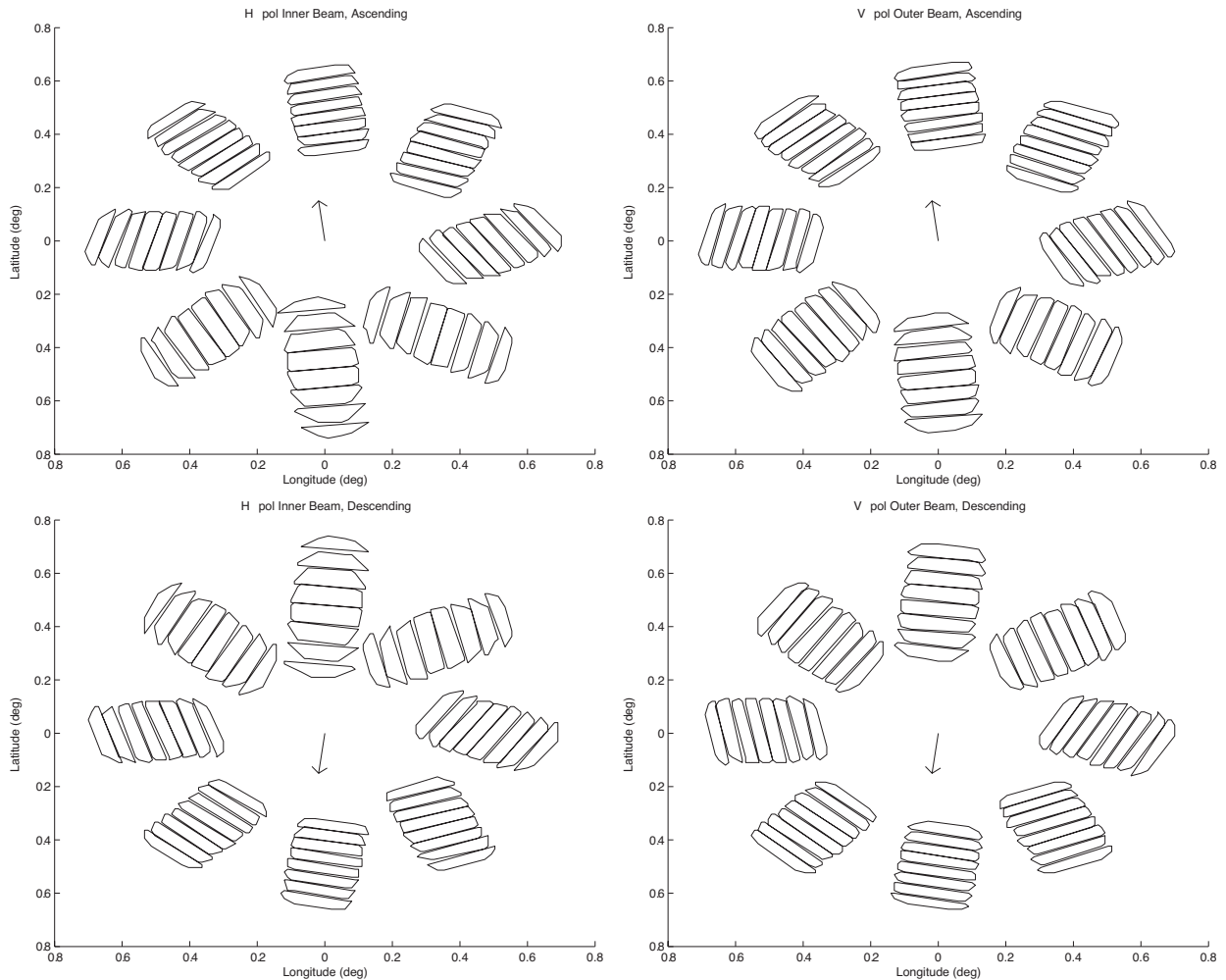


**Figure 3.** Illustration of the variation in slice shape for the inner and outer beams at ascending and descending crossings of the equator versus the antenna azimuth angle. The 3 dB slice contours are shown. The 8 slices corresponding to a given measurement are shown at 8 antenna azimuth angles.

Computation of the spatial response  $h$  requires detailed knowledge of the antenna pattern ( $G$ ), the operation of the on-board processor ( $G_F$  and the Doppler shift pre-compensation), and the observation geometry which determines  $R$  and the  $x$  and  $y$  coordinate system. As these parameters vary with antenna azimuth angle and orbit position,  $h$  varies with these parameters, significantly complicating computation and storage of  $h$ . This is particularly the case for slices. Figure 3 illustrates the variation in slice  $h$  with antenna azimuth angle and orbit position. The computer code used to compute  $h(x, y)$  is part of the code used for computation of the SeaWinds  $X$  factor<sup>7</sup> (see Eq. 8).

Since computation of the spatial response is complex and computationally intensive, a lookup table-based approach can be used for computing and storing  $h$ . With care, such an approach is simple, efficient and accurate. A method for tabulating the SeaWinds egg and slice response functions has been developed. It is described below. The tables for computing the spatial response for both eggs and slices along with accompanying code are available online at <http://scp.byu.edu> under “Software” and “SeaWinds Xshape” links.

The tabularized spatial responses provide  $h(x, y)$  where the spatial  $x, y$  coordinates are converted to longitude  $u$  and latitude  $v$  perturbation terms. These are added to the nominal longitude and latitude reported

in the standard JPL/SeaWinds L1B measurement center locations, i.e. the absolute location is the sum of the  $u, v$  perturbations computed from the tables and the measurement center location. The tabularization and computation methods are different for eggs and slices. Note that while slices offer the highest resolution, slice  $\sigma^\circ$  measurements are noisier than egg  $\sigma^\circ$  measurements since the eggs offer more averaging.

### 3.1. Slice response function

As previously noted, the slice response can be quantized to 1 within the 3 dB response and 0 outside of it,

$$h(x, y) = \begin{cases} 1 & \text{if } (x, y) \text{ is in the contour} \\ 0 & \text{otherwise.} \end{cases}$$

Thus, all that is required is a description of the 3 dB contour line. While the contour is a continuous curve, for compact storage and ease of use, the contour is modeled by eight key ‘‘corner’’ points connected by straight lines. This yields reconstruction of the contour to sufficient accuracy (compare the slice shapes in Figs. 2 and 3 which show continuous slice contours and approximate, ‘‘cornered’’ contours, respectively). The location of these points relative to the measurement are tabulated based on the slice number, the orbit time and azimuth angle. A separate table is used for each digital processor resolution mode. The table contains rotation angles, the vector difference in location between the various corner points and the slice center at each azimuth angle, and orbit locations for each slice. For a given antenna azimuth angle  $\psi$  and orbit location determined by the orbit-time (time in seconds from the ascending equator crossing time)  $t$ , the table is interpolated to compute the slices.

Extracting the slice corners from the table and converting to latitude and longitude includes three basic steps. First, the azimuth rotation angle  $\phi$  table is linearly interpolated based on the antenna azimuth angle and orbit position. Note that this interpolation must properly handle the  $0^\circ$ - $360^\circ$  transition. Then, the  $x, y$  point position table is linearly interpolated in antenna azimuth rotation angle and orbit time. Each corner point is then rotated on the grid using

$$\begin{bmatrix} \tilde{x} \\ \tilde{y} \end{bmatrix} = \begin{bmatrix} \cos(\phi) & \sin(\phi) \\ -\sin(\phi) & \cos(\phi) \end{bmatrix} \begin{bmatrix} x \\ y \end{bmatrix}.$$

Finally, each  $\tilde{x}, \tilde{y}$  corner point is converted to latitude ( $v$ ) and longitude ( $u$ ) using

$$u = \frac{\tilde{x}}{r_2} + u_0$$

and

This equation should read  $v = \arcsin\left(\frac{y - \left(1 - \cos\left(\frac{x}{r_2}\right)\right) \sin(v_0) r_2}{r}\right) + v_0$

$$v = \arcsin\left(\tilde{y} - \left(1 - \cos\left(\frac{\tilde{x}}{r_2}\right)\right) \sin(v_0) \frac{r_2}{r}\right) + v_0$$

where  $v_0$  and  $u_0$  are the latitude and longitude respectively of the slice center as reported in the JPL L1B data product. In this equation  $r$  is the local radius of the Earth approximated by

$$r = (1 - F \sin^2(v_0)) R_E$$

where  $F = 3.3528 \times 10^{-6}$ ,  $R_E = 6378.1$  km and

$$r_2 = r \cos(v_0).$$

Lines connecting the resulting 8 points describe the approximate shape of the 3 dB contour of the spatial response function in longitude and latitude.

For use in imaging, the corner points are transformed from latitude and longitude via geometric projection onto the imaging grid. The resulting 8-sided figure is then row scanned to determine which image pixels the measurement overlaps. Figure 4 illustrates the pixelization of slice contour onto the imaging grid.

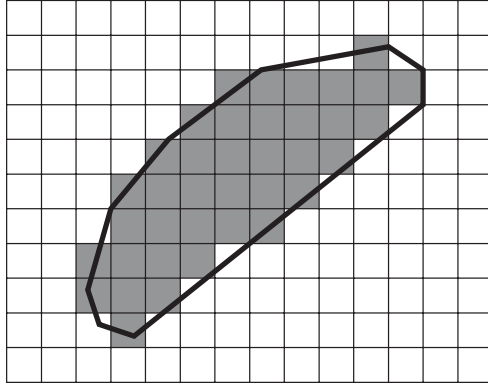


**Figure 4.** Illustration of a tabularized 3 dB slice contour overlaying an imaging grid. Imaging grid pixels whose centers are contained within the slice contour are shaded to indicate which pixels the slice is considered to have “covered” in the image. Alternate choices of which pixels “belong” to the contour can also be used. See Long et al.<sup>4</sup>

### 3.2. Egg response function

The eggs are tabulated by azimuth angle and orbit time similar to the slices. However for the eggs, a multidimensional polynomial in the latitude and longitude perturbation is employed,

$$h(\tilde{u}, \tilde{v}) = \sum_{i=0}^N \sum_{j=0}^{N-i} a_{ij} \tilde{u}^i \tilde{v}^j$$

where  $\tilde{u}$  and  $\tilde{v}$  are the longitude and latitude deltas to be added to the egg center longitude  $u_0$  and latitude  $v_0$  and the  $a_{ij}$  parameters stored in the table. Thus,  $u = \tilde{u} + u_0$  and  $v = \tilde{v} + v_0$ . A second order polynomial is used where  $N = 2$ . Separate tables are created for each digital processor resolution mode. The egg response in latitude and longitude is computed by linearly interpolating the  $a_{ij}$  coefficients in azimuth angle and orbit time and then evaluating  $h(u, v)$  at the desired locations.

In imaging, the latitude and longitudes corresponding to the imaging pixel centers are determined and  $h(u, v)$  computed for each pixel. Typically, a cutoff (e.g., -10 dB) is employed, below which  $h$  is set to zero.

## 4. APPLICATION EXAMPLES

The dominant application of the SeaWinds tabularized spatial responses is creating images of the surface backscatter. Thus, we provide a short discussion on creating images from SeaWinds backscatter. Such images are used for a variety of purposes, including climate change studies, sea ice monitoring, iceberg tracking, and hurricane tracking.<sup>2</sup> SeaWinds backscatter images are provided to the public via the Scatterometer Climate Record Pathfinder project <http://www.scp.byu.edu>. These applications are facilitated by the use of reconstruction and resolution enhancement of the SeaWinds backscatter measurements.

The SeaWinds orbit geometry, antenna rotation, and pulse repetition frequency combine to result in a dense sampling of spatially overlapping measurements (see Fig. 5). This dense, overlapping sampling is exploited by reconstruction algorithms such as the Scatterometer Image Reconstruction<sup>3,4</sup> algorithm to reconstruct the  $\sigma^\circ$  of the surface at finer effective spatial resolution than the 3 dB size of the individual  $\sigma^\circ$  measurements. While spatial resolution enhancement is possible for single beams in single look directions, combining measurements from different look directions and/or multiple passes significantly improves the effective sampling density and, hence, the spatial resolution reconstruction capability. Note that separate images of vertically- and horizontally-polarized  $\sigma^\circ$  are created.

To illustrate how spatially overlapping measurements can provide improved effective spatial resolution, consider Fig. 6. In this example, two simplified slice-like measurements are defined. These have long, thin

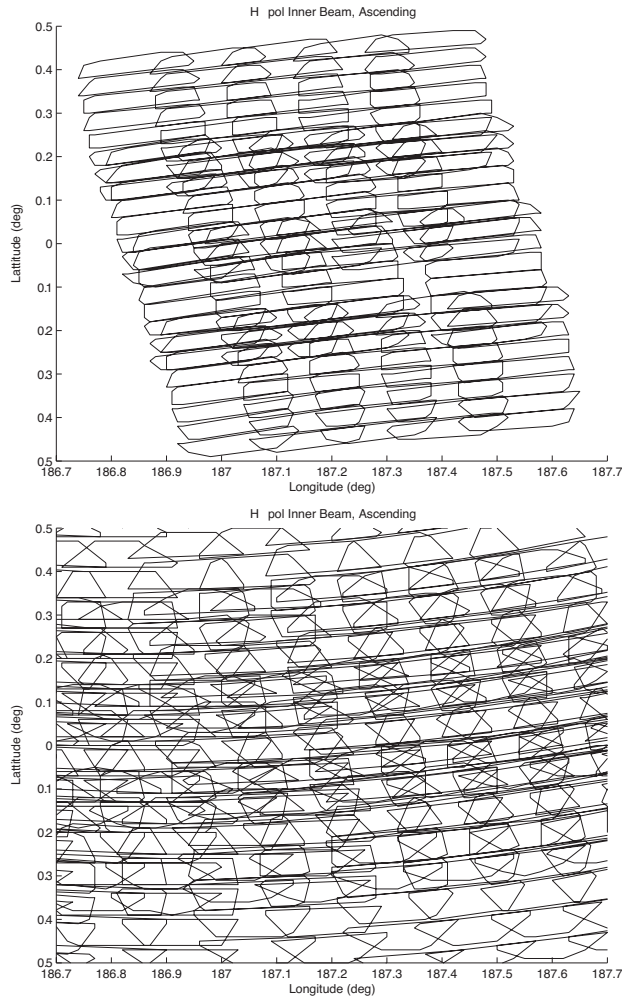


**Figure 5.** Illustration of the inner beam (H-pol) slice sampling near the equator for several pulses and antenna rotations on a single ascending pass. (top) Forward-looking measurements. (bottom) Aft-looking measurements.

response functions which have dissimilar orientations. The orientation variations result from rotation of the antenna for SeaWinds. One measurement results from a forward-facing measurement, while the second results from a backward-facing measurement. (The relative orientation varies over the swath, however.) When the overlapping measurements are averaged, we find that the 3 dB resolution is a smaller, centralized area compared to the larger 3 dB contour of the individual measurements, thus providing improved spatial resolution. Coupling this effect with the inverse filter inherent in the reconstruction<sup>3</sup> results in further improvements in the effective resolution.

Because the slice measurements have finer intrinsic resolution and higher sampling density than the egg measurements, they facilitate better image reconstruction. However, the slice measurements are also noisier. Since reconstruction tends to enhance the noise along with the resolution, there is a tradeoff between noise and resolution. Figure 7 compares the imaging resolution of egg and slice measurements. The improvement in effective resolution when using reconstruction and enhancement is clear, as is the improvement in slice resolution over egg resolution. A comparison of SeaWinds and ERS-1/2 reconstruction is shown in Ref.<sup>3</sup>



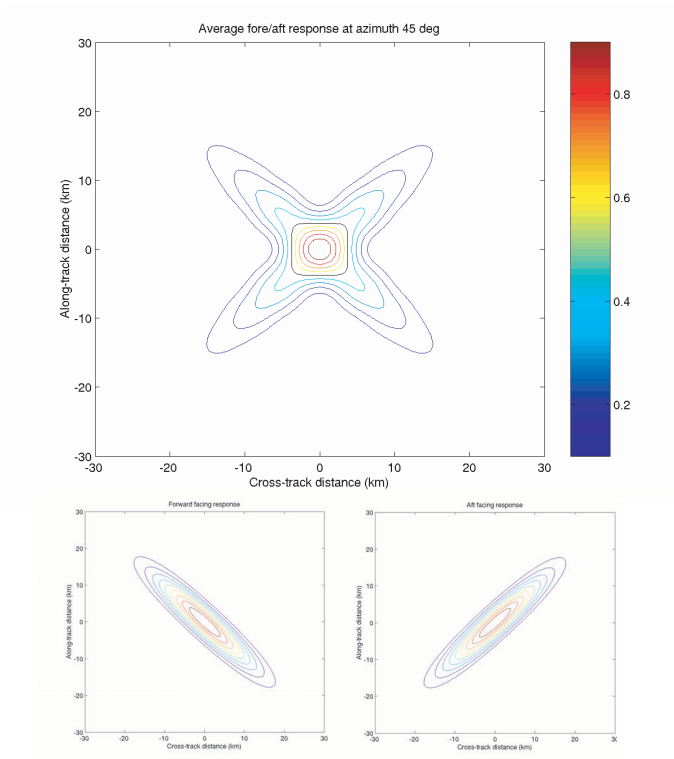


**Figure 6.** Illustration of how combining overlapping measurements can yield improved spatial resolution. The spatial response from two simplified slice-type measurements are shown in the bottom, reduced-size plots. The top figure shows the effective spatial response when the two measurements are averaged. See the text for further explanation.

## 5. CONCLUSIONS

The spatial response function of remote sensing radar measurements is required when using the measurements in resolution and imaging algorithms. It can also be useful in studies where multiple measurements are combined or in studies of beam filling effects. Computation of the SeaWinds spatial response function, which varies between beam and with antenna rotation position is laborious. We have provided a brief description of our method for tabularizing the spatial response function of SeaWinds backscatter measurements and some of the issues which arise in developing and using the tabularized response function. We hope that by providing this information to the public we can further the use of SeaWinds data in studies of the Earth.

## ACKNOWLEDGMENTS

SeaWinds data was obtained from the Physical Oceanography Distributed Data Archive (PO.DAAC) at the CalTech Jet Propulsion Laboratory.

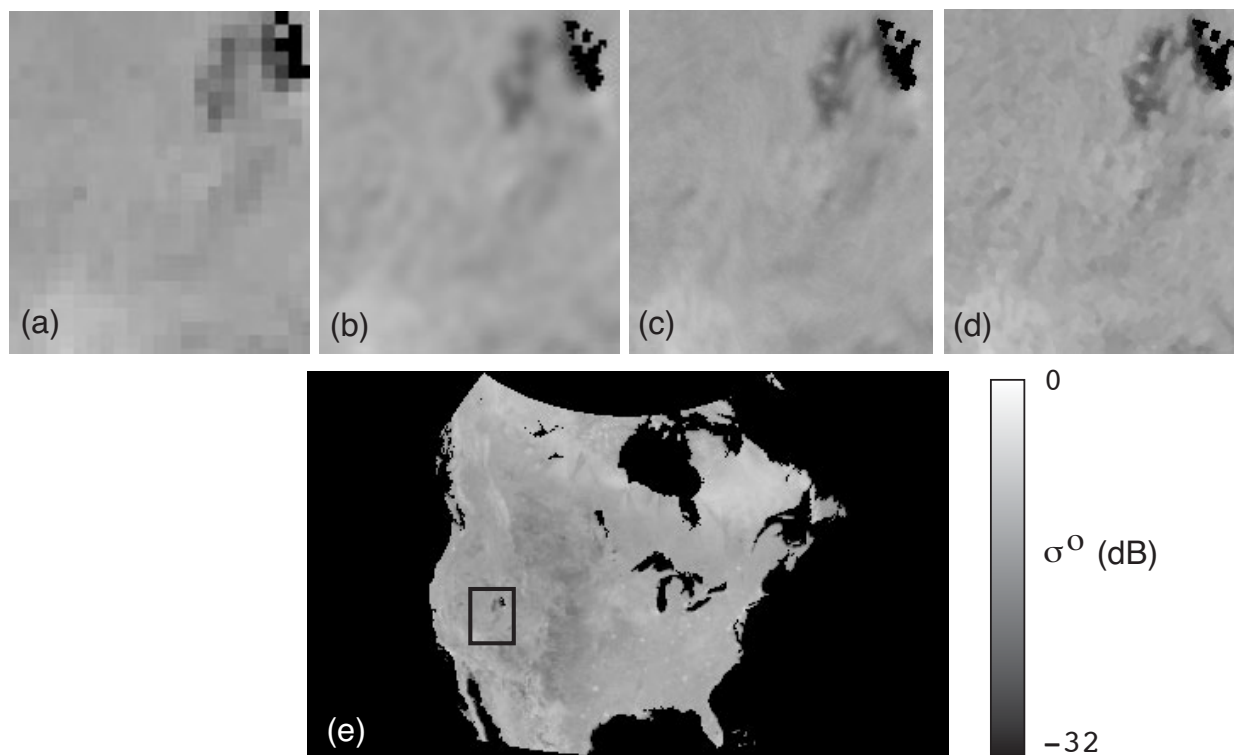


**Figure 7.** Comparison of SeaWinds backscatter images (in dB) created from slices and eggs using various reconstruction algorithms. The top row shows a study area over Utah and Nevada. The Great Salt Lake has been masked out. The dark patch left of the Great Salt Lake (the dark patch in the upper right) is the West Desert Salt Flats, including the Bonneville Salt Flats. (a) Egg measurements gridded onto a 25 km resolution grid. Each pixel consists of the average of all egg measurements whose center fall within the pixel area. This imaging method does not require a description of the spatial response, but provides the coarsest effective resolution. (b) Image created using the SIR algorithm from egg measurements using the polynomial shape description. (c) Image created from slices using the “AVE” algorithm.<sup>4</sup> Pixel values are computed as the average of all measurements which “cover” this pixel. (d) Image created using the SIR algorithm from slice measurements using the tabularized 3 dB contour description. (e) Image of North America highlighting the study area.

## REFERENCES

1. F. Naderi, M. Freilich, and D. Long, “Spaceborne radar measurement of wind velocity over the ocean—an overview of the NSCAT scatterometer system,” *Proc. IEEE* **79**(6), pp. 850–866, 1991.
2. D. Long, M. Drinkwater, B. Holt, S. Saatchi, and C. Bertoia, “Global ice and land climate studies using scatterometer image data,” *EOS, Trans. American Geophysical Union* **82**(43), p. 503, 23 Oct. 2001.
3. D. Early and D. Long, “Image reconstruction and enhanced resolution imaging from irregular samples,” *IEEE Trans. Geosci. Remote Sens.* **39**(2), pp. 291–302, 2001.
4. D. Long, P. Hardin, and P. Whiting, “Resolution enhancement of spaceborne scatterometer data,” *IEEE Trans. Geosci. Remote Sens.* **31**(3), pp. 700–715, 1993.
5. M. Spencer, C. Wu, and D. Long, “Improved resolution backscatter measurements with the SeaWinds pencil-beam scatterometer,” *IEEE Trans. Geosci. Remote Sens.* **38**(1), pp. 89–104, 2000.
6. F. Ulaby, R. Moore, and A. Fung, *Microwave Remote Sensing: Active and Passive*, vol. 2, Artech House, Inc., Norwood, Massachusetts, 1986.
7. I. Ashcraft, D. Long, A. Anderson, S. Richards, M. Spencer, and B. Jones, “Sigma-0 retrieval from SeaWinds on QuikSCAT,” in *Earth Observing Systems IV*, W. L. Barnes, ed., *Proc. SPIE* **3750**, pp. 171–179, 1999.